


RESEARCH

Open Access



The 2019 *Mw* 7.0 Banten, Indonesia, intraslab earthquake: investigation of the coseismic slip, tsunami modelling and Coulomb stress change

Endra Gunawan^{1*} , Widjo Kongko², Munawar Kholil³, Bayu Triyogo Widyantoro³, Sri Widiyantoro^{1,4}, Pepen Supendi⁵, Nuraini Rahma Hanifa⁶, Ira Mutiara Anjasmara⁷, Cecep Pratama⁸ and Aditya Riadi Gusman⁹

Abstract

The 2019 *Mw* 7.0 Banten, Indonesia, earthquake occurred at a 49 km depth in a relatively unknown region, where the geological structure did not clearly show the fault. In this study, we use the Global Navigation Satellite System data to analyse the fault source of the earthquake. Following the earthquake's focal mechanism, we modelled a total of four fault models using two possible fault strikes, with each of the fault strikes investigated for shallow top depth and deeper top depth. This study also utilises the tide gauge data to confirm the tsunami waveform, modelled using the estimated coseismic slip. We present evidence of the shallow rupture of the 2019 *Mw* 7.0 Banten, Indonesia, intraslab earthquake from an ENE-WSW fault direction. The tsunami modelling of a shallow top depth of an ENE-WSW fault direction is a better fit in predicting the tide gauge waveform. We also present evidence that the 2019 Banten intraslab earthquake generated very few aftershocks for a magnitude 7-class earthquake. The stress transfer of a shallow rupture ENE-WSW fault model was able to explain the relocated two weeks of aftershocks.

Keywords: Coseismic slip, 2019 Banten intraslab earthquake, GNSS, Tsunami, Aftershocks, Coulomb stress change

Introduction

On 2 August 2019, 12:03 UTC at a ~50 km distance off the coast of Banten, Indonesia, a damaging *Mw* 7.0 earthquake occurred as a result of tectonic activity between the Australian Plate and the Sunda Block in this particular region (Fig. 1; Bock et al. 2003; DeMets et al. 2010). Following the earthquake, four people died and more than 200 houses were damaged or destroyed, as reported by the Indonesian National Board for Disaster Management (BNPB). Shaking was felt up to southern Sumatra and western Java.

The United States Geological Survey (USGS) reported that the 2019 Banten earthquake epicentre was relatively deep at 49 km depth. The focal mechanisms of the

earthquake suggest two possible fault source directions. The first possible fault was an ENE-WSW fault direction with a strike of 69° and dip to the south. The other possible fault was dipping to the west of an NEN-SWS fault direction with a strike of 201°. The subsurface seismic profile obtained by seismic data did not clearly show the fault that could have ruptured during the event in this particular region (Susilohadi et al. 2009). Thus, the fault responsible for the 2019 Banten earthquake is not well-known.

In order to address this issue, this study investigated four fault models responsible for the 2019 Banten earthquake using two possible fault strikes, with each of the fault strikes investigated for shallow top depth and deeper top depth. The distribution of the subsurface coseismic slip during the 2019 Banten earthquake was inferred using Global Navigation Satellite System (GNSS) data available from the Indonesian Continuously Operating Reference Stations (Ina-CORS)

*Correspondence: endra.gunawan@itb.ac.id

¹ Global Geophysics Research Group, Faculty of Mining and Petroleum Engineering, Bandung Institute of Technology, Bandung, Indonesia
Full list of author information is available at the end of the article

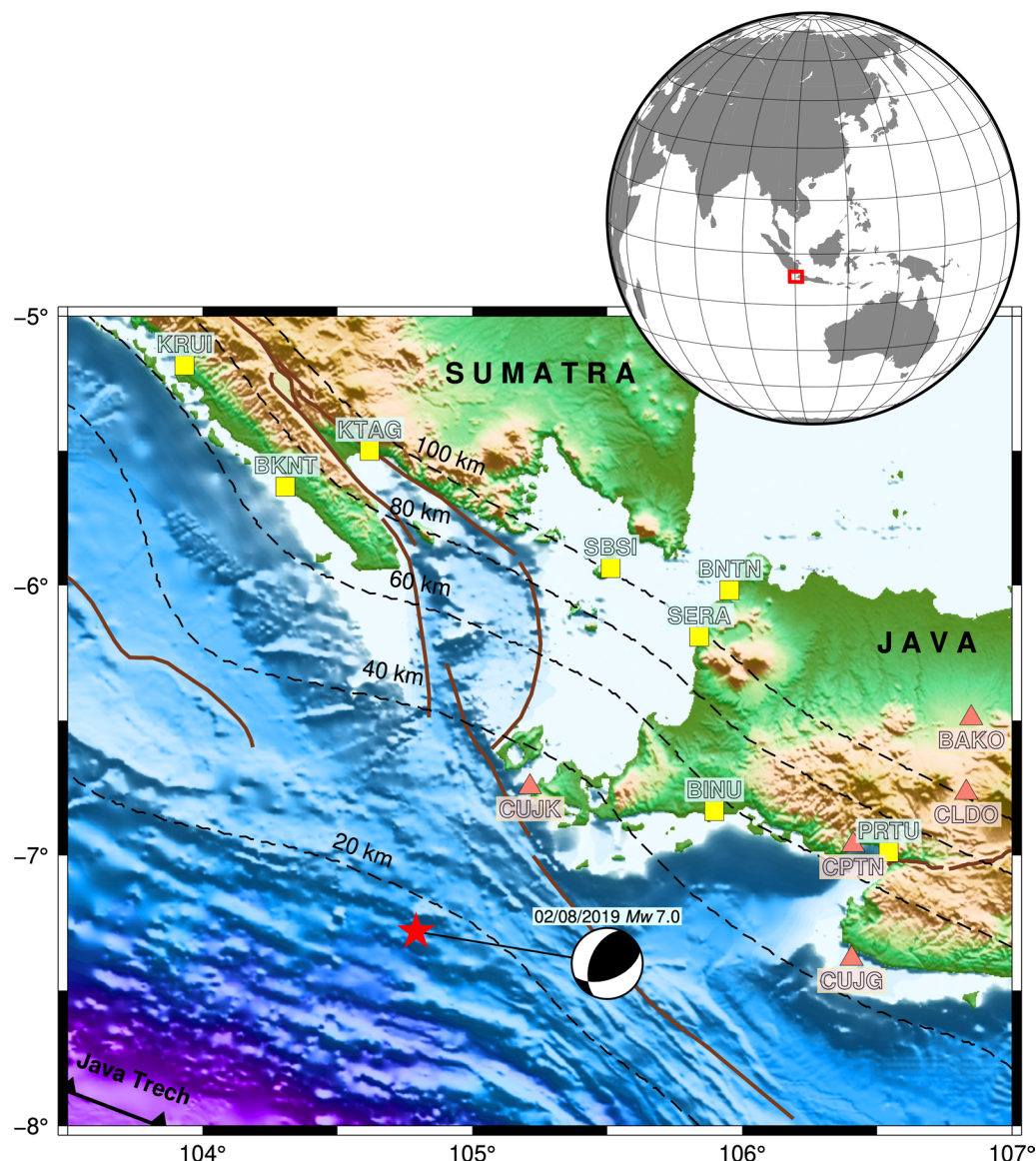


Fig. 1 Tectonic setting of this study. The red star indicates the location of the 2019 Banten earthquake, with focal mechanism from USGS. The light red colour triangles show the locations of GNSS stations, while the yellow squares indicate the location of the tide gauge. Dashed lines denote depth of slab. Brown lines remarks active faults obtained from Gunawan (2021). Bathymetry and topography are taken from SRTM15+ (Tozer et al. 2019). The inset shows the larger regional setting

network maintained by the Indonesian Geospatial Information Agency (BIG). We also modelled the tsunami waveform using the estimated coseismic slip of four models and compared it with the tide gauge data available along the coast of southern Sumatra and western Java (Fig. 1). Finally, we also investigated the Coulomb stress transfer and compared it with the relocated aftershocks from the Indonesian Agency for Meteorology, Climatology and Geophysics (BMKG) network.

Materials and methods

In this study, we utilise GNSS data, tidal observation data, and aftershocks data to investigate the fault responsible for the 2019 Banten earthquake. The information of this data and the methodology used in this study are described below.

GNSS

The GNSS data used by this study was obtained from the Indonesia Continuously Operating Reference Station

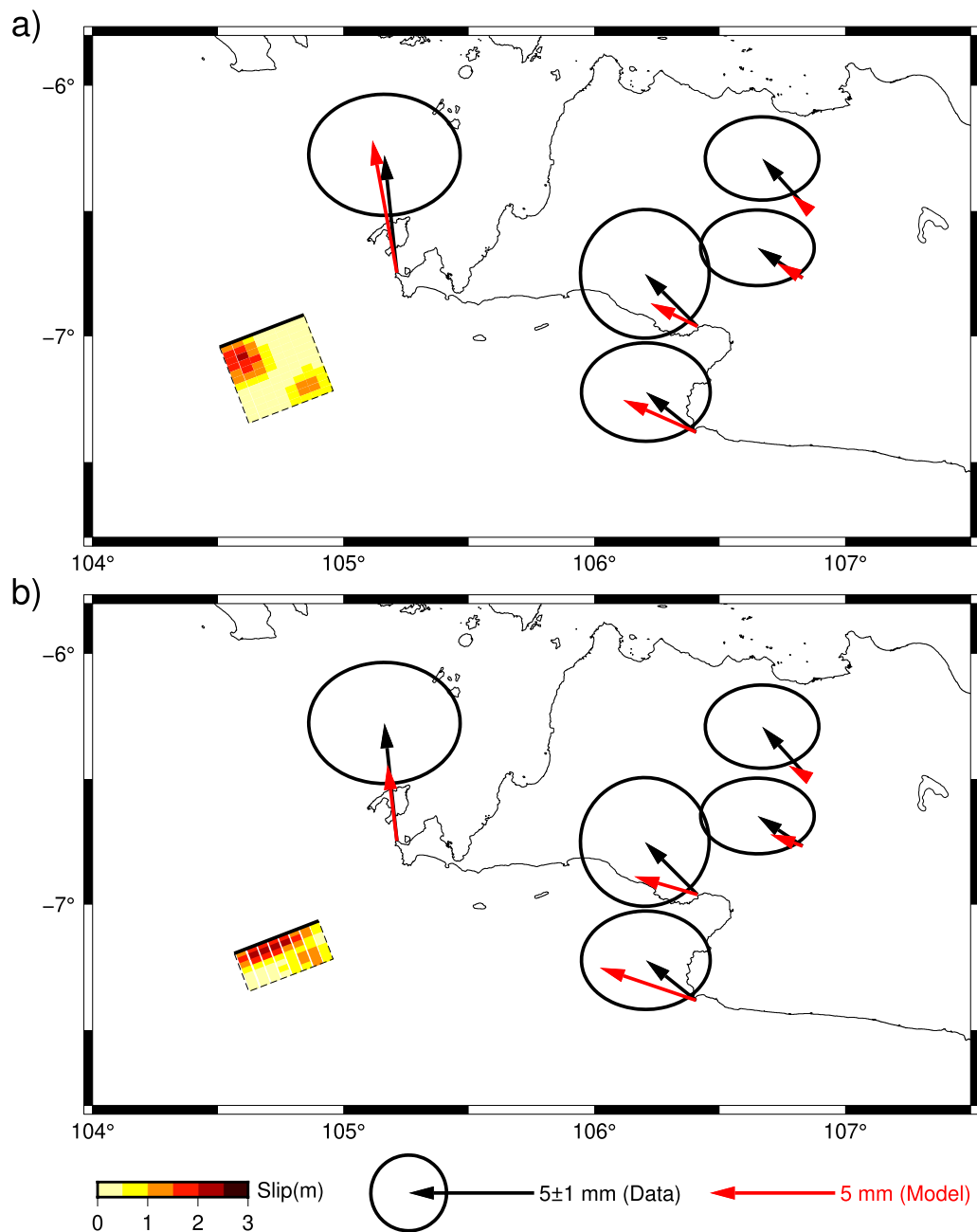


Fig. 2 Coseismic slip inversion results for **a** Model 1A; **b** Model 1B. The black vectors indicate the GNSS data used in the inversion, while the red vectors show the displacement models. The solid black line delineates the top of the fault

(Ina-CORS) (Gunawan et al. 2019; Gunawan and Widiyantoro 2019), which was available during the 2019 Banten earthquake event. The GNSS antennae of the Ina-CORS station are located embedded on top of a concrete structure. The GNSS data, which is recorded with a 30-s sampling interval, was processed using GipsyX software

(Bertiger et al. 2020) and GAMIT software (Herring et al. 2010), described below.

During daily solution estimation using GipsyX, we conducted static solutions in the precise point positioning mode. We employed fiducial-free with five iterations and JPL's reanalysis final set of the International GNSS

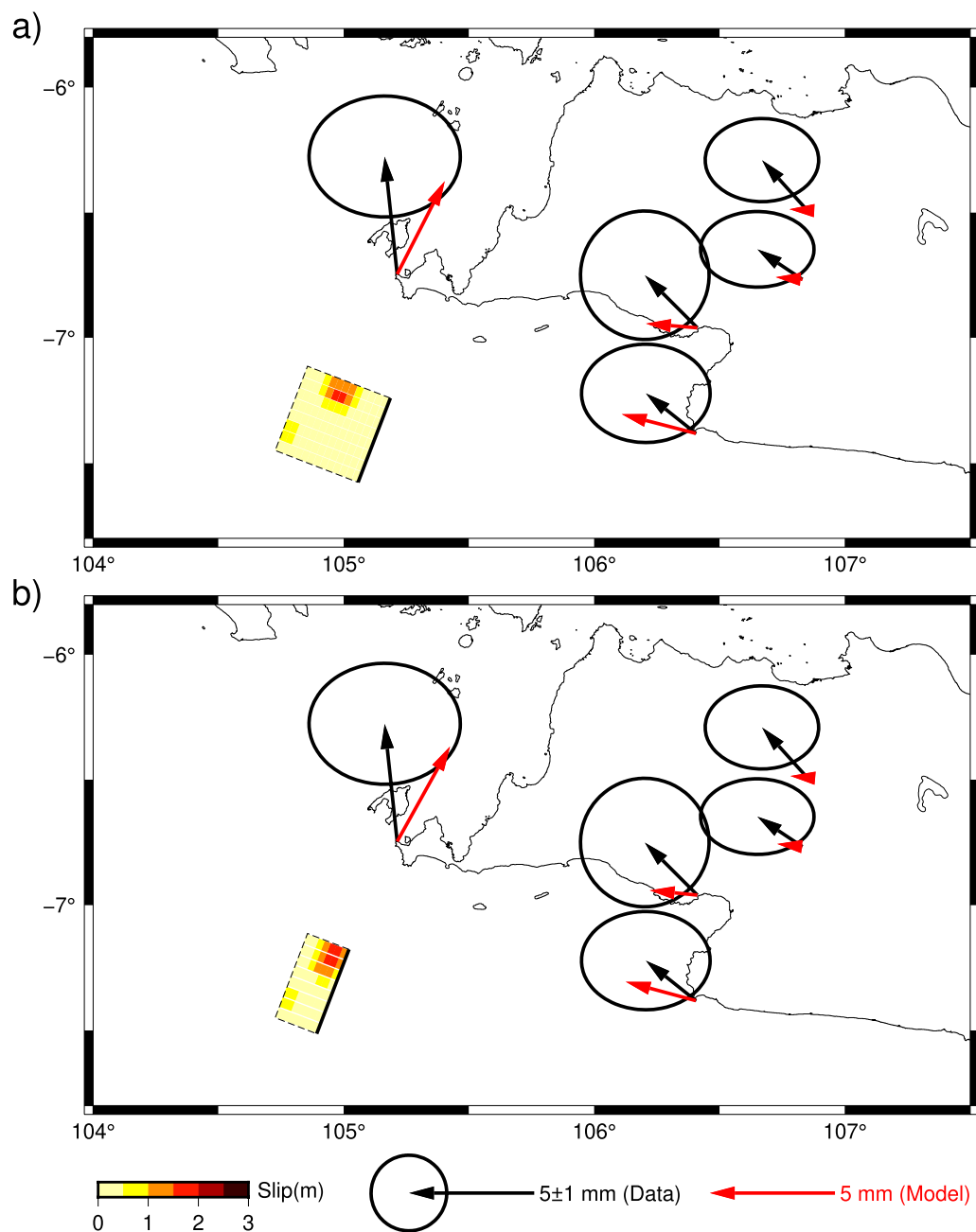


Fig. 3 Coseismic slip inversion results for **a** Model 2A; **b** Model 2B. (See Fig. 2 for a detailed description of the figure legend)

Service 2014 (IGS14) orbit and clock product. Ocean loading parameters were obtained from the Onsala Space Observatory (<http://holt.oso.chalmers.se/loading/>) using the GOT4.8 model. In addition, we also set an elevation angle cut-off with 15°.

Meanwhile, our daily solution estimation used GAMIT incorporating processing steps as used by Gunawan et al. (2021). First, the daily position was estimated with atmospherically used, loose-constraint, prior GNSS phase

observations; the orbit and earth-orientation parameters were fixed. Second, these positions and their covariance with global GNSS solutions, computed as part of Massachusetts Institute of Technology's processing for the International GNSS Service (IGS), were combined. Third, the clarified position time series were estimated. In both the second and third steps, the loosely constrained solution was mapped onto a well-constrained reference frame by minimising the position and velocity differences of

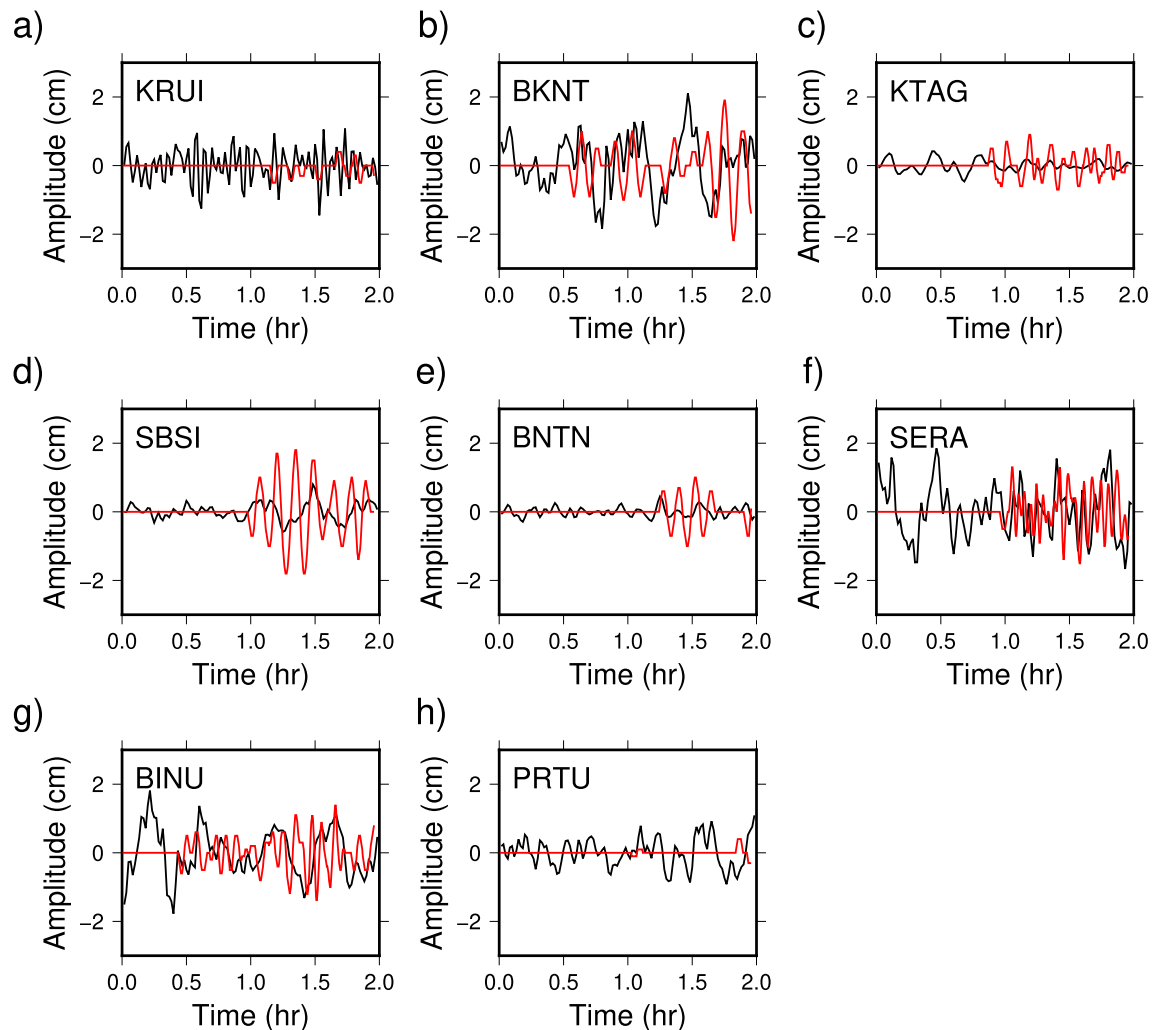


Fig. 4 Tide gauge data record and waveform model of fault Model 1A at each tide gauge station. The data after filtering using a de-tiding and moving average process are shown by the black line. The waveform model of fault Model 1A is shown by the red line. The tide gauge stations are: **a** KRUI, **b** BKNT, **c** KTAG, **d** SBSI, **e** BNTN, **f** SERA, **g** BINU, and **h** PRTU

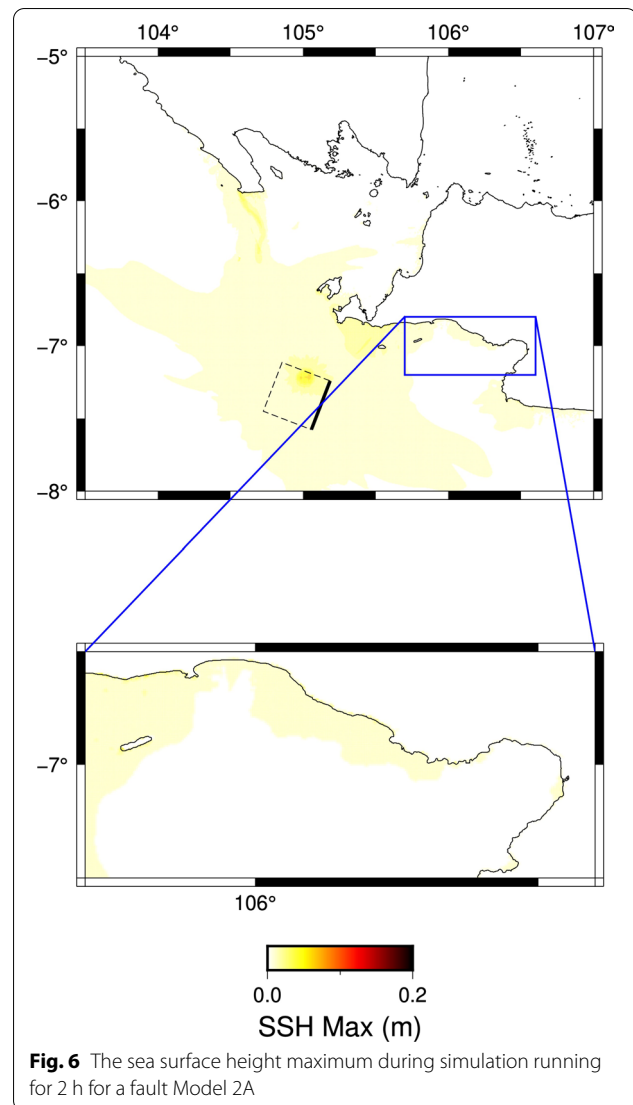
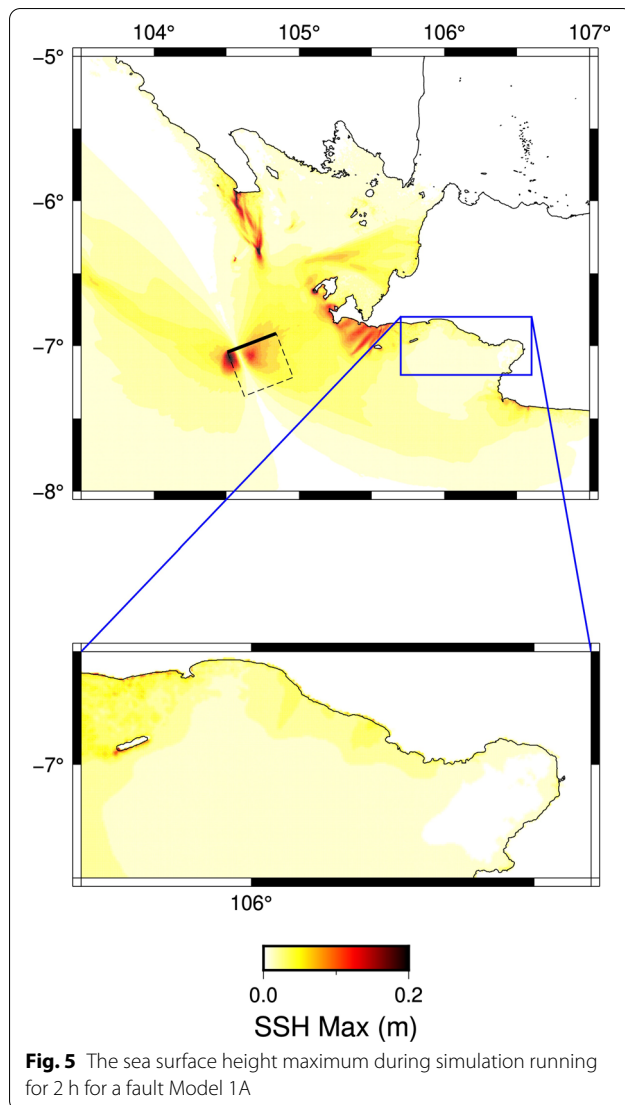
selected stations with respect to a priori values defined by the IGS14 realisation of the International Terrestrial Reference Frame (ITRF) 2014 reference frame.

Using the processed daily solutions GNSS data, we extracted the coseismic displacements by subtracting the velocity data for five days after the earthquake to five days before the earthquake. For each coseismic displacement analysis process obtained from GipsyX and GAMIT, we took the average value and used it as final coseismic displacements of the 2019 Banten earthquake.

Coseismic slip inversion

The coseismic slip inversion was calculated using the final coseismic displacements obtained from the

processed GNSS data. In our search for the fault model of the 2019 Banten earthquake, we modelled using two possible fault strikes based on the earthquake focal mechanism as reported by the USGS. The first fault strike model, named Model 1, dips to the south of an ENE-WSW fault direction with a strike of 69° . The second fault strike model, named Model 2, dips to the west of a NEN-SWS fault direction with a strike of 201° . The dip angle for Model 1 is 54° , while the dip angle for Model 2 is 49° . In both models, the length of the fault is 40 km, which is estimated using an earthquake scaling relationship for dip-slip faulting system (Gunawan 2021). We also divided the main fault into sub-faults with a length and width of 5 km.

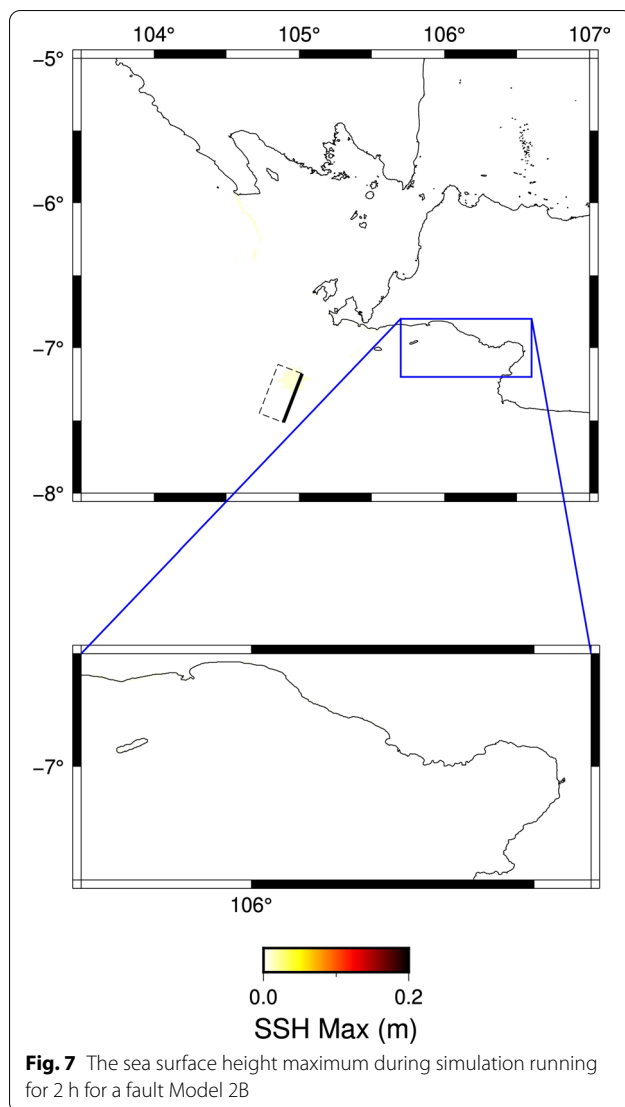


In our inversion, we utilised *sdm2013* (Wang et al. 2011; 2013) to estimate the coseismic slip distribution. This process follows the objective function as follows: $F(m) = \|Gm - d\|^2 + \alpha^2 \|H\tau\|^2$. In this function, G is the Green's functions obtained from an elastic half-space model (Okada 1992), m is a coseismic slip of each sub-fault, d is coseismic displacements, α^2 is the smoothing factor, which controlled by the model roughness and data misfit, H is the finite difference approximation of the Laplacian operator, and τ is the shear stress drop. For every fault model, we investigated using a shallow top fault depth of 1 km, hereinafter referred to as Model 1A and Model 2A, and a deep top fault depth of 25 km, hereinafter referred to as Model 1B and Model 2B. All of the four models were constructed with a bottom depth of 50 km.

Tsunami

In this study, we modelled the tsunami waveform using the estimated coseismic slip of those four models (Models 1A, 1B, 2A and 2B) and compared it with the tide gauge data available along the coast of southern Sumatra and western Java. The tidal observation data was obtained from the national tide gauge stations network operated by BIG. Eight tide gauge stations located off the coasts of western Java and southern Sumatra were used to understand the possible tsunami waveform as recorded by the tide gauge. The location of these tide gauge stations is shown in Fig. 1.

To extract the probable tsunami waveform recorded by the tide gauge, first, we conducted a de-tiding process to separate the data from its tidal components. In this process, we used a bandpass filter FFT (Fast Fourier Transformation) with a period of 3 to 30 min (Rabinovich 1997;



Heidarzadeh and Satake 2013). Then, although the tide component was removed, the recorded data may suffer interference from noise. To eliminate this type of noise, the tide gauge data was then filtered using the moving averages process. In this study, a moving average was carried out for 15 pieces of data, or for tide gauge data with a 1-min sampling rate of 15 min.

The tsunami modelling was performed with the use of TSUNAMI-N3. The model data and setup were as follows. First, the numerical domain for this study was in the boundary of geographic coordinates in longitude between 103°E and 107°E, and latitude between 5°S and 8°S. The geometric data used GEBCO Compilation Group (2020) combined with a navy chart provided by the BNPB. The grid data used in this study was set to be

450 m, and the simulation time for this model was 7200 s or 2 h.

Aftershocks

Aftershocks obtained from the Indonesian Agency for Meteorology, Climatology and Geophysics (BMKG) network were used to understand the possibility that the mainshock raised stress in the surrounding region and triggered these aftershocks. We relocated aftershocks using a Double-Difference (DD) method (Waldhauser and Ellsworth 2000). In this method, when the hypocentre distribution distance between two earthquakes is very small compared to the distance between the source station, then the ray-path and waveform of the two earthquakes can be considered to be approximately the same. With this assumption, the difference in travel time between the two earthquakes recorded at the same station can be considered only as a function of the distance between the two hypocentres.

Pesicek et al. (2010) developed the DD method for teleseismic cases by adapting the P wave beam tracking method for the case of spherical earth (Koketsu and Sekine 1998). We used the DD method for the teleseismic distance, named *teletomoDD*, which uses a nested regional-global 3D velocity model (Widiyantoro and van der Hilst 1997). For regional models, the 3D velocity model is used and for the global model, the AK135 velocity model is used (Kennett et al. 1995).

Results and discussion

Coseismic slip

Our estimation of the final coseismic displacements of the 2019 Banten earthquake suggests that the GNSS stations located closest to the epicentre, CUJK, experience coseismic displacements of ~5 mm. Meanwhile, the farthest GNSS stations, BAKO, experience ~3 mm. The estimated coseismic displacements of the 2019 Banten earthquake at GNSS stations in western Java are shown in Figs. 2 and 3.

Following our coseismic slip inversion, Model 1A and Model 1B suggest that the high slip is located in the shallower part of the design fault geometry, where ~2.0 m slip of Model 1A is located at 11 km depth and ~2.4 m slip of Model 1B is located at 30 km depth (Fig. 2). We calculated a misfit between GNSS data displacement and model displacement using mean absolute error as follows: $MAE = 1/n \sum_{i=1}^n (data_i - model_i)$. Our investigation for the Model 1A indicated that the misfit is 2 mm, while in the Model 1B it is 3 mm. Meanwhile, high coseismic slip of Model 2A is ~1.5 m at 24 km depth, while Model 2B is ~2.0 at 30 km depth (Fig. 3). Misfit from Model 2A and Model 2B are ~4 mm, which is higher than Model 1A and Model 1B. Using 30 GPa as rigidity, Model

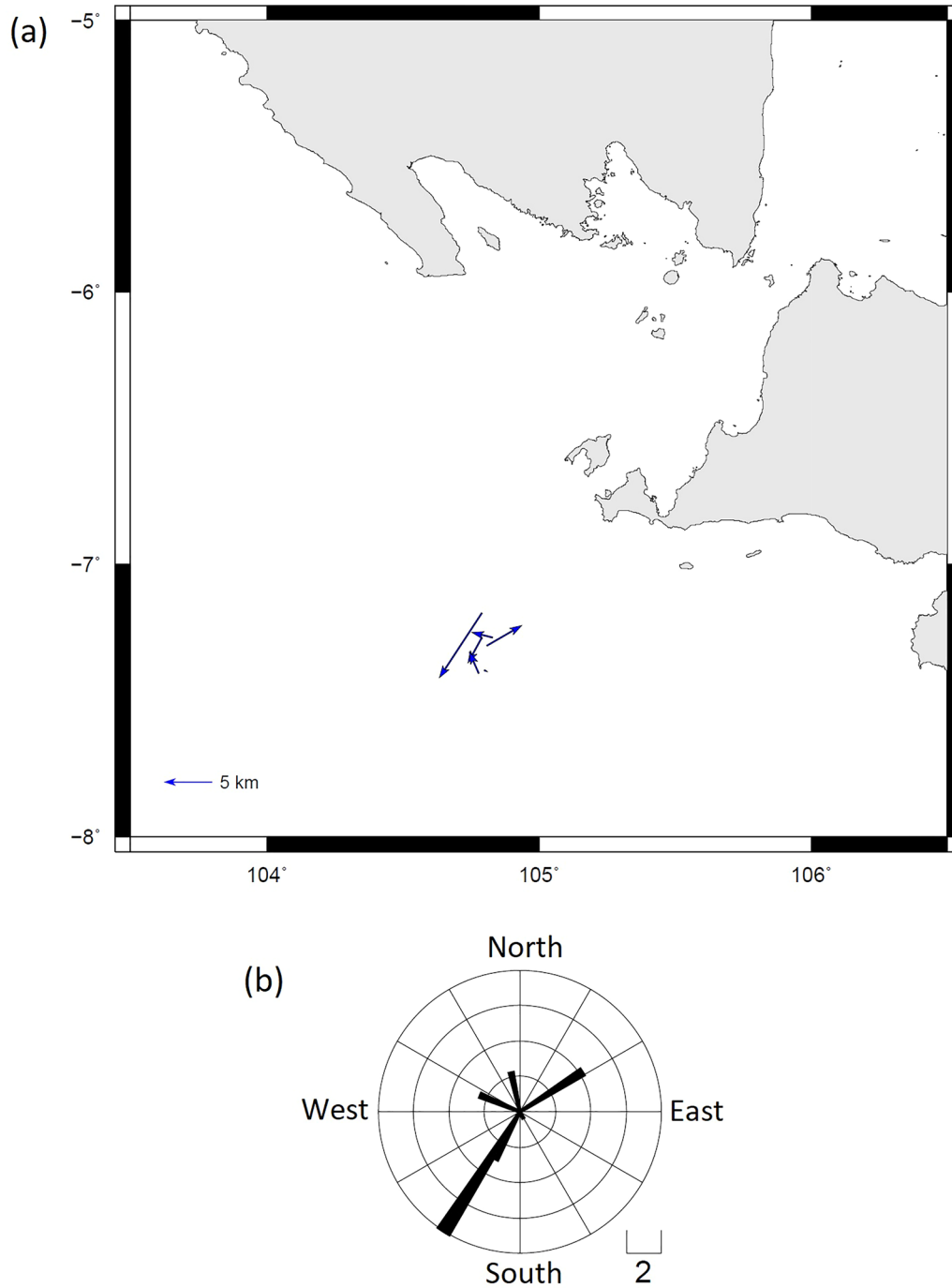
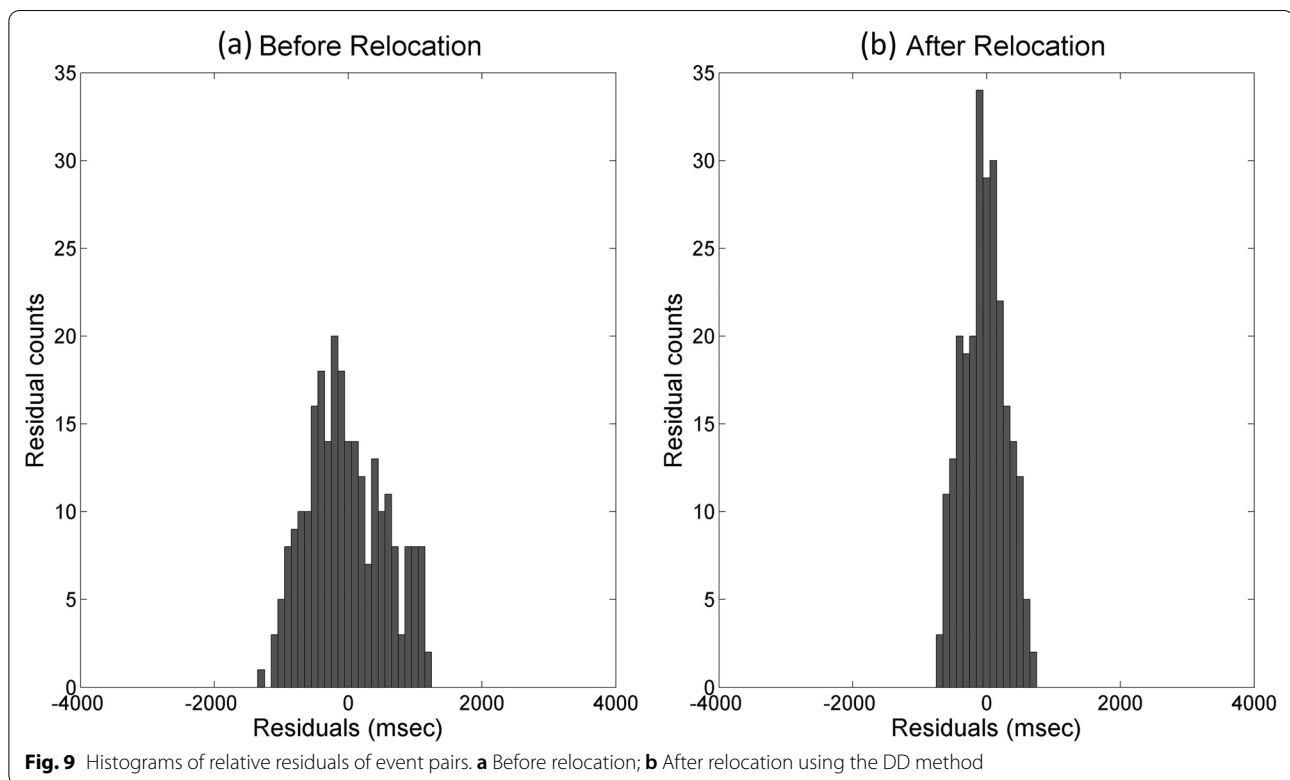


Fig. 8 **a** Epicenter shifts of the DD locations relative to the BMKG catalog; **b** Rose diagram showing the dominant direction of relocation shifts

1A and Model 1B yield geodetic moment of 4.22×10^{19} N m and 3.95×10^{19} N m, which are both equivalent with M_w 7.0. Meanwhile, Model 2A and Model 2B yield a geodetic moment of 1.90×10^{19} N m and of 2.00×10^{19} N m, which are both equivalent with M_w 6.80.

Tsunami modelling

Figure 4 shows the tide gauge record after being filtered using the de-tiding and moving average process. Tsunami waveforms at the tide gauges are simulated using each of the estimated coseismic slip models. The simulated tsunami waveforms are then compared with the observed



one to find the best earthquake source model. The vertical surface displacement for the tsunami simulation is calculated from the estimated coseismic slip model using the equations in Mansinha and Smylie (1971). The Model 1A generated highest sea surface height (SSH) maximum compared to the other three models (Fig. 5). Our results also suggest that the Model 1B did not generate a tsunami, while the sea surface heights of Model 2A (Fig. 6) and Model 2B (Fig. 7) were very small and did not reach the tide gauge stations. Our tsunami modelling of these four fault models indicates that a significant tsunami occurs when the fault is ruptured at a shallow depth of the fault.

Comparing the tsunami waveform from each fault model and the tide gauge data, we found that tsunami waveform of fault Model 1A is comparable and better fits the tide gauge data than the other model, although it is important to note that the waveform amplitude is very small, only ~ 2 cm. With such a small amplitude, a noticeable comparison of the tsunami ~ 1 h after the mainshock was detected at SBSI and BNTN. At some tide gauge stations however, such as SERA and BINU, early 30 min tide gauge data still contained noise which could not be removed. This most likely happened because these stations are located at a pier, harbour, or bay, with a relatively shallow depth of < 15 m, thus data is influenced by the beach morphology.

Coulomb stress change

Using the BMKG network, we recorded only one earthquake event with magnitude 4.2, which occurred on 3 August 2019 at 22 km of depth, and three magnitude 3-class earthquakes, which occurred on 6 August 2019. Between 6 and 15 August 2019, no aftershock was recorded. Then, another aftershock with M_w 3.9 occurred on 16 August 2019. Figures 8 and 9 shows epicenter shifts of the DD locations relative to the BMKG catalog and the histograms of relative residuals of event pairs. Thus, during the two weeks after the mainshock, only five aftershocks of the 2019 Banten earthquake were recorded. This is fewer than after the 2006 M_w 7.8 Java tsunami earthquake which occurred in the shallow interplate or forearc region (Bilek and Engdahl 2007).

Using the relocated aftershocks, we investigated the possibility that the mainshock raised stress in the surrounding region and triggered aftershocks. We calculated the Coulomb stress change as follows: $\Delta CFF = \Delta\tau + \mu'\Delta\sigma$, where $\Delta\tau$ is the shear stress change on a given fault plane (positive in the direction of receiver fault slip), $\Delta\sigma$ is the fault normal stress change (positive for fault unclamping) and μ' is the effective fault friction coefficient on the receiver fault (Toda et al. 1998, 2011; Gunawan et al. 2018). Positive values of ΔCFF indicate

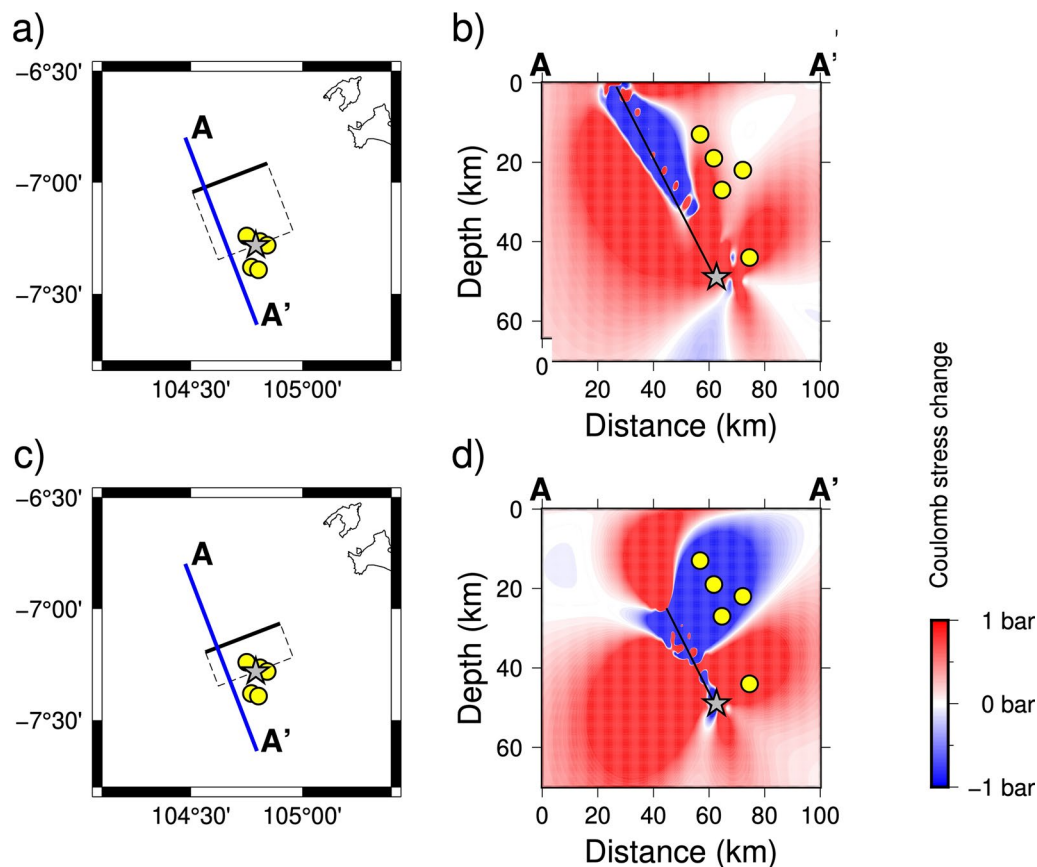


Fig. 10 Relocated aftershocks distribution from 3—16 August 2019 and Coulomb stress change analysis correspond with fault **a, b** Model 1A, **c, d** Model 1B. **a, c** Distribution of the relocated aftershocks are shown by yellow circles; **b, d** The vertical view of calculated Coulomb stress change along profile AA'

that the stress in a region is acting to promote slip, negative values suggest opposition to slip.

Using $\mu' = 0.8$, we found that the correlation between positive values of ΔCFF with aftershocks location fit well for fault Model 1A (Fig. 10b). For the other models, aftershocks were located in the negative values of ΔCFF (Figs. 10d, 11b, d). The ΔCFF investigation supports the preferences fault model from the minimum misfit of GNSS data displacement and model displacement obtained by the fault Model 1A and the tsunami modelling.

Our investigation suggests that the 2019 Banten earthquake occurred on an ENE-WSW fault direction, where the fault ruptured at a shallow depth. The GNSS data inversion, stress transfer analysis and tsunami modelling support this hypothesis. The geophysical survey conducted in this particular region, however, did not identify an ENE-WSW structure, which was responsible for the 2019 Banten earthquake (Susilohadi et al. 2009). This happened because the geophysical survey line (SO 137-27 in Fig. 2 of Susilohadi et al. 2009) is parallel to the

fault structure responsible for the 2019 Banten intraslab earthquake.

Our findings emphasise the need for further improvement of the geophysical data collection through marine geophysical survey, additional continuous GNSS and seismic stations in Java, especially towards a better understanding of any future potential earthquakes that may occur in Java. Widiyantoro et al. (2020) proposed a locking megathrust in southern Java with an estimated magnitude of M_w 9.1 if all segments in Java are ruptured. Utilising comprehensive data would be very useful to identify the earthquake source in Java, especially in performing disaster mitigation to reduce risk in this most populated island in Indonesia.

Conclusion

We investigated the 2 August 2019 M_w 7.0 Banten intraslab earthquake using GNSS data available in western Java. We estimated the coseismic slip of fault models with the direction of ENE-WSW and

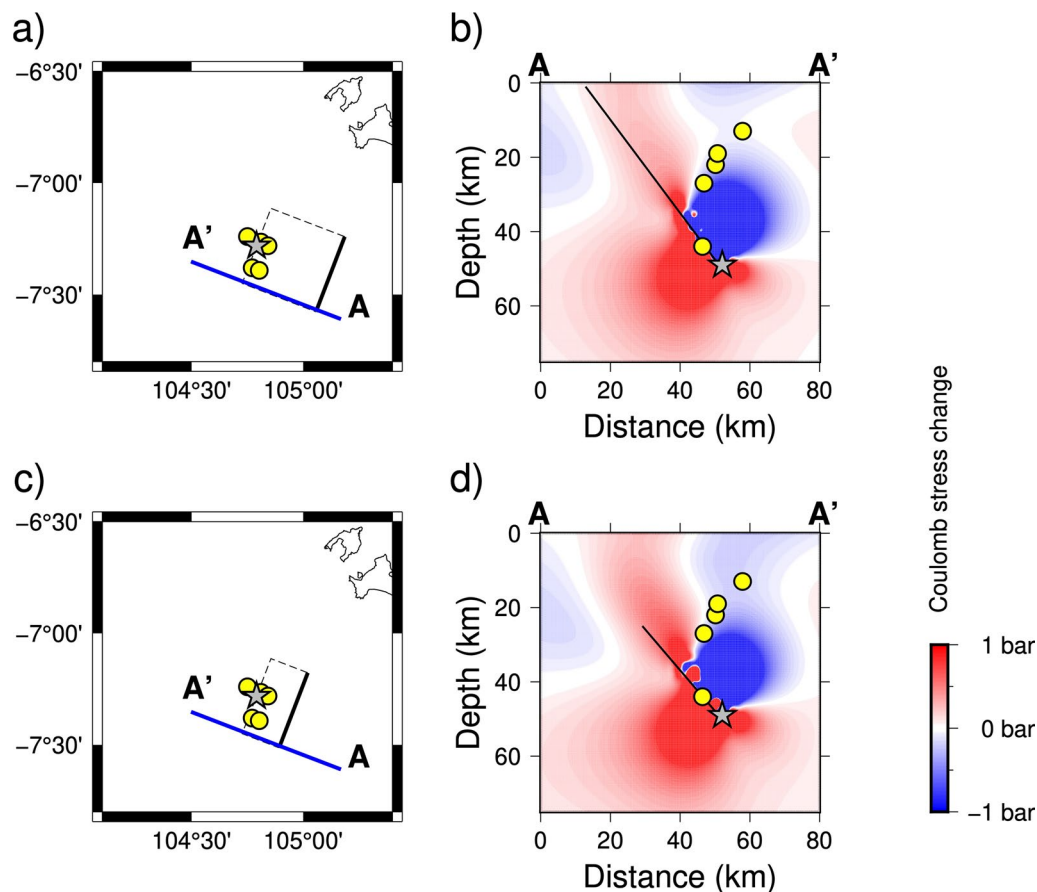


Fig. 11 Relocated aftershocks distribution from 3–16 August 2019 and Coulomb stress change analysis correspond with fault **a, b** Model 2A, **c, d** Model 2B. (See Fig. 10 for a detailed description of the figure legend)

NEN-SWS. In every fault direction, two fault models were investigated with shallow top depth and deeper top depth. We show that the minimum misfit between GNSS data displacement and model displacement was obtained from our modelling using an ENE-WSW fault direction. The fault models with the direction of NEN-SWS poorly predict displacement nearest to the epicentre. Using the coseismic slip estimation, we conducted tsunami modelling on each of the model and compared the result with the tide gauge data. We showed that tsunami modelling of a shallow top depth of an ENE-WSW fault direction is a better fit in predicting the tide gauge waveform. Finally, we also found that the stress transfer of a shallow rupture ENE-WSW fault model was able to explain the relocated two weeks of aftershocks. Our investigation suggests that the 2019 Mw 7.0 Banten, Indonesia, intraslab earthquake ruptured on a shallow portion of the fault with an ENE-WSW direction. Performing disaster mitigation through identification of earthquake source is very crucial, considering Java is

the most populated island in Indonesia and prone to future potential megathrust earthquakes.

Abbreviations

GNSS: Global Navigation Satellite System; ENE-WSW: East North East-West South West; BNPB: Indonesian National Board for Disaster Management; USGS: United States Geological Survey; NEN-SWS: North East North-South West South; Ina-CORS: Indonesian Continuously Operating Reference Stations; BIG: Indonesian Geospatial Information Agency; BMKG: Indonesian Agency for Meteorology, Climatology and Geophysics; IGS: International GNSS Service; ITRF: International Terrestrial Reference Frame; FFT: Fast Fourier Transformation; DD: Double-Difference; MAE: Mean Absolute Error.

Acknowledgements

The authors would like to thank the Editor, Christopher Gomez, and two anonymous reviewers for the thoughtful comments, which help improve the quality of this manuscript. We also thank BMKG and BIG for providing the earthquake data and GNSS data used in this study. Figures were generated using Generic Mapping Tools (GMT) software (Wessel et al. 2019).

Author contributions

EG: conceptualization, investigation, writing, methodology, discussion, review and editing, WK and ARG: tsunami analysis, writing, methodology and discussion, MK: GNSS processing, BTW: tide gauge processing, SW and PS: seismic analysis, writing, methodology and editing, NRH, IMA and CP: conceptualization and discussion. All authors read and approved the final manuscript.

Funding

This study is partially supported by the 2022 National Research Priority of National Research and Innovation Agency, the Indonesian Collaborative Research Program and the Overseas Research Grants of The Asahi Glass Foundation.

Availability of data and materials

The datasets used and analysed during the current study are available from the corresponding author on reasonable request.

Declarations

Competing interests

The authors declare that they have no competing interests.

Author details

¹Global Geophysics Research Group, Faculty of Mining and Petroleum Engineering, Bandung Institute of Technology, Bandung, Indonesia. ²Laboratory for Harbor Infrastructure and Coastal Dynamics Technology, National Research and Innovation Agency, Yogyakarta, Indonesia. ³Geospatial Information Agency, Cibinong, Indonesia. ⁴Faculty of Engineering, Maranatha Christian University, Bandung, Indonesia. ⁵Agency for Meteorology, Climatology and Geophysics, Bandung, Indonesia. ⁶Research Center for Geological Disaster, National Research and Innovation Agency, Bandung, Indonesia. ⁷Department of Geomatics Engineering, Sepuluh Nopember Institute of Technology, Surabaya, Indonesia. ⁸Department of Geodetic Engineering, Gadjah Mada University, Yogyakarta, Indonesia. ⁹GNS Science, Lower Hutt, New Zealand.

Received: 20 October 2021 Accepted: 26 May 2022

Published online: 10 June 2022

References

- Bertiger W, Bar-Sever Y, Dorsey A, Haines B, Harvey N, Hemberger D, Heflin M, Lu W, Miller M, Moore AW, Murphy D (2020) GipsyX/RTGx, a new tool set for space geodetic operations and research. *Adv Space Res* 66(3):469–489
- Bilek SL, Engdahl ER (2007) Rupture characterization and aftershock relocations for the 1994 and 2006 tsunami earthquakes in the Java subduction zone. *Geophys Res Lett* 34(20)
- Bock Y, Prawirodirdjo L, Genrich JF, Stevens CW, McCaffrey R, Subarya C, Puntodewo SSO, Calais E (2003) Crustal motion in Indonesia from global positioning system measurements. *J Geophys Res Solid Earth* 108(B8)
- DeMets C, Gordon RG, Argus DF (2010) Geologically current plate motions. *Geophys J Int* 181(1):1–80
- GEBCO Compilation Group (2020) GEBCO 2020 grid. <https://doi.org/10.5285/a29c5465-b138-23a4de053-6c86abc040b9>
- Gunawan E (2021) An assessment of earthquake scaling relationships for crustal earthquakes in Indonesia. *Seismol Res Lett*. <https://doi.org/10.1785/0220200267>
- Gunawan E, Widiyantoro S (2019) Active tectonic deformation in Java, Indonesia inferred from a GPS-derived strain rate. *J Geodyn* 123:49–54. <https://doi.org/10.1016/j.jog.2019.01.004>
- Gunawan E, Widiyantoro S, Rosalia S, Daryono MR, Meilano I, Supendi P, Ito T, Tabei T, Kimata F, Ohta Y, Ismail N (2018) Coseismic slip distribution of the 2 July 2013 Mw 6.1 Aceh, Indonesia, earthquake and its tectonic implications. *Bull Seismol Soc Am* 108(4):1918–1928. <https://doi.org/10.1785/0120180035>
- Gunawan E, Widiyantoro S, Marliyani GI, Sunarti S, Ida R, Gusman AR (2019) Fault source of the 2 September 2009 Mw 6.8 Tasikmalaya intraslab earthquake, Indonesia: analysis from GPS data inversion, tsunami height simulation, and stress transfer. *Phys Earth Planet Inter* 291:54–61. <https://doi.org/10.1016/j.pepi.2019.04.004>
- Gunawan E, Kholil M, Widiyantoro S (2021) Coseismic slip distribution of the 14 January 2021 Mamuju-Majene, Sulawesi, earthquake derived from GPS data. *Nat Hazards*. <https://doi.org/10.1007/s11069-021-05084-y>
- Heidarzadeh M, Satake K (2013) The 21 May 2003 tsunami in the Western Mediterranean Sea: statistical and wavelet analyses. *Pure Appl Geophys* 170(9–10):1449–1462
- Herring TA, King RW, McClusky SC (2010) GAMIT reference manual release 10.4, Report. Massachusetts Institute Technology, Cambridge, pp 1–171
- Kennett BL, Engdahl ER, Buland R (1995) Constraints on seismic velocities in the Earth from traveltimes. *Geophys J Int* 122(1):108–124
- Koketsu K, Sekine S (1998) Pseudo-bending method for three-dimensional seismic ray tracing in a spherical earth with discontinuities. *Geophys J Int* 132(2):339–346
- Mansinha LA, Smylie DE (1971) The displacement fields of inclined faults. *Bull Seismol Soc Am* 61(5):1433–1440
- Okada Y (1992) Internal deformation due to shear and tensile faults in a half-space. *Bull Seismol Soc Am* 82(2):1018–1040
- Pesicek JD, Thurber CH, Zhang H, DeShon HR, Engdahl ER, Widiyantoro S (2010) Teleseismic double-difference relocation of earthquakes along the Sumatra-Andaman subduction zone using a 3-D model. *J Geophys Res Solid Earth* 115(B10)
- Rabinovich AB (1997) Spectral analysis of tsunami waves: Separation of source and topography effects. *J Geophys Res Oceans* 102(C6):12663–12676
- Susilohadi S, Gaedicke C, Djajadihardja Y (2009) Structures and sedimentary deposition in the Sunda Strait. *Indonesia Tectonophysics* 467(1–4):55–71
- Toda S, Stein RS, Reasenberg PA, Dieterich JH, Yoshida A (1998) Stress transferred by the 1995 Mw = 6.9 Kobe, Japan, shock: effect on after-shocks and future earthquake probabilities. *J Geophys Res Solid Earth* 103(B10):24543–24565
- Toda S, Stein RS, Lin J (2011) Widespread seismicity excitation throughout central Japan following the 2011 Mw = 9.0 Tohoku earthquake and its interpretation by Coulomb stress transfer. *Geophys Res Lett* 38(7)
- Tozer B, Sandwell DT, Smith WHF, Olson C, Beale JR, Wessel P (2019) Global bathymetry and topography at 15 arc sec: SRTM15+. *Earth Space Sci* 6(10):1847–1864
- Waldhauser F, Ellsworth WL (2000) A double-difference earthquake location algorithm: method and application to the northern Hayward fault, California. *Bull Seismol Soc Am* 90(6):1353–1368
- Wang R, Schurr B, Milkereit C, Shao Z, Jin M (2011) An improved automatic scheme for empirical baseline correction of digital strong-motion records. *Bull Seismol Soc Am* 101(5):2029–2044
- Wang R, Parolai S, Ge M, Jin M, Walter TR, Zschau J (2013) The 2011 Mw 9.0 Tohoku earthquake: comparison of GPS and strong-motion data. *Bull Seismol Soc Am* 103(2B):1336–1347
- Wessel P, Luis JF, Uieda L, Scharroo R, Wobbe F, Smith WHF, Tian D (2019) The generic mapping tools version 6. *Geochem Geophys Geosyst*. <https://doi.org/10.1029/2019GC008515>
- Widiyantoro S, van der Hilst R (1997) Mantle structure beneath Indonesia inferred from high-resolution tomographic imaging. *Geophys J Int* 130(1):167–182
- Widiyantoro S, Gunawan E, Muhari A, Rawlinson N, Mori J, Hanifa NR, Susilo S, Supendi P, Shiddiqi HA, Nugraha AD, Putra HE (2020) Implications for megathrust earthquakes and tsunamis from seismic gaps south of Java Indonesia. *Sci Rep* 10:15274. <https://doi.org/10.1038/s41598-020-72142-z>

Publisher's Note

Springer Nature remains neutral with regard to jurisdictional claims in published maps and institutional affiliations.